Increased drought and pluvial risk over California due to changing oceanic conditions

Jonghun Kam and Justin Sheffield

Department of Civil and Environmental Engineering, Princeton University, Princeton, 08544

First submission to the *Expedited Contribution* section of *Journal of Climate*

August 2015

First resubmission to *Journal of Climate*

May 2016

Second resubmission to *Journal of Climate*

August 2016

Corresponding author (currently):
Dr. Jonghun Kam
The Atmospheric and Oceanic Program
Princeton University
Princeton, NJ, 08540
USA
tel: +1-609-452-5352
fax: +1-609-987-5063
email: jkam@princeton.edu

Abstract

We evaluate winter-time drought and pluvial risk over California through a Bayesian analysis of the upper and lower quartile of PRISM-based precipitation from 1901-2015. Risk is evaluated for different time windows to estimate the impact of inter-annual and decadal-to-multidecadal Pacific and Atlantic variability (positive and negative phases of ENSO, PDO, and AMO). The impact of increasing trends in global sea surface temperature (SST) on drought and pluvial risk, is also examined with idealized experimental runs from three climate models (GFDL-AM2.1, CCM3.0, and GFS). The results shows that the influence of oceanic conditions on drought risk in California is significant but has changed with higher risk in the last half century, especially in southern California. The influence of oceanic conditions on pluvial risk has also been significant, especially during the warm phase of the Pacific Ocean, but increases over the last century are small compared to drought. Results from the idealized climate model experiments show that natural variability likely played a major role in the observed changes in risk, with the global SST increasing trend possibly tempering the increases regionally but not significantly over California. Despite evolving preferential oceanic conditions for a pluvial event during the 2015/16 winter (positive phase of ENSO and PDO), California received an 11% winter precipitation surplus, which was not sufficient for drought recovery. The seasonal and longer-term outlook for negative phases of the ENSO and PDO implies that drought risk will be elevated in southern California for the next decade.

1. Introduction

California is one of the most vulnerable states in the U.S. to severe drought due to the large and growing water demand for irrigation, energy production, and recreation, and the limited water supply from the relatively dry regional climate (Grantham and Viers 2014). The current drought that has persisted since 2011 has led to a declaration of a drought state of emergency and mandatory curtailment of municipal and agricultural water use (Seager et al. 2015). Most of California's precipitation falls in the wintertime and the current drought has been driven by reductions in precipitation over the past winters (Mao et al. 2015). The data record (Daly et al. 2008) shows record-breaking deficits in December 2013 and January 2014 relative to the past century, moderate deficits in February 2014, and significant total winter precipitation deficits (<25th percentile) during 2013/14 winter (Figure 1c). Most of California (67% of the state) experienced some form of severe drought (below 25th percentile) during the winters of 2011-14. The drought was also compounded by the more moderate impact of warming induced declines in snowpack and earlier snowmelt, which has affected the state water supply and water temperatures in the following seasons (Barnett et al. 2008). Snowfall in the Sierra Nevada Mountains at the mid- February 2015 was the lowest since 1951 (Mao et al. 2015; Pan et al. 2003) and below the 10th percentile at the end of February 2015 (Figure 1a). These deficits led to reduced groundwater recharge and combined with continued groundwater pumping, especially in the highly productive agricultural region of the Central Valley (Figure 1b), drove groundwater depletion of about 2 mm/year (about 70% of the regional total water loss) since 2003 (Famiglietti et al. 2011). Precipitation during the last winter (2014-15) was slightly above the 25th percentile but was not enough for drought recovery.

Although the current drought is exceptional in terms of its impacts, there have been multiple severe and often lengthy droughts over the last century and before. These include, the severe but short winter drought of 1976/77 (Namias 1978) and longer-term dry conditions during 1987-1992 (Dixon et al. 1996). Prior to the instrumental record, paleoclimate data indicate that the region has experienced droughts that dwarf anything experienced during the past century, including 'mega-droughts' during the mediaeval period (Stine 1994; Cook et al. 2014).

The physical mechanisms that lead to drought for the region are complex (Namias 1978; Schubert et al. 2004) and are complicated further by the potential influence of climate change (Seager et al. 2007) that may be changing the risk of drought. About 45% of California's annual precipitation occurs in winter, and originates mainly from advected moisture via westerly winds over the extra-tropical Pacific Ocean (Gimeno et al. 2012). In turn, this is driven by variations in the Pacific as characterized by the El Niño Southern Oscillation (ENSO; Schonher and Nicholson, 1989) and Pacific Decadal Oscillation (PDO; McCabe et al. 2004), and modulated by conditions in the north Atlantic depending on the season, shifting the location of the North American jet and the position and strength of the wave train (Mo et al. 2009). Several studies have shown an influence of global warming on California winter precipitation across spatial scales. At the planetary scale, the current California drought has been influenced by a reduction in North Pacific storms due to the presence of upper-level high-pressure anomalies over the east North Pacific (Bond et al. 2015). These in turn have been linked to the record-breaking warm sea surface temperature anomalies over that region in 2014, the risk of which has been estimated to be amplified about two times by anthropogenic impacts (Kam et al. 2015). On the other hand global warming has been implicated in the increase in the risk of pluvials over California (Wang and Schubert 2014) due to increases in atmospheric humidity over the eastern North Pacific. The current drought has also been linked to the recent global warming hiatus (Delworth et al. 2015).

This study is designed to understand the influence of oceanic conditions on drought and pluvial risk over California and its changes from observational data and to evaluate the impact of global sea surface warming trends on risk. To meet this purpose, this study uses a Bayesian approach to compute drought and pluvial risk during the full period, and during positive and negative phases of the PDO, AMO, and ENSO. We also use data from idealized experimental runs from three global climate models (GFDL-AM2.1, CCM3.0, and GFS). Detailed descriptions of the data and methods are presented in section 2. Section 3 shows the resulting drought and pluvial risk maps over California from the observational data, as well as the GCM-simulated precipitation deficit and surplus forced by prescribed SST anomaly patterns with and without SST trends. Section 4 highlights the findings of this study and provides an outlook for California drought and pluvial risk.

2. Data and Methods

The annual PDO, AMO, and Southern Oscillation Index (SOI) indices for 1900-2014 were computed from monthly indices from the University of Washington, NOAA Earth System Research Laboratory, and the Bureau of Meteorology, Australian Government, respectively. The SOI index is of the opposite sign of ENSO. Wintertime precipitation values over California for 1901-2015 were computed from monthly precipitation data from the Parameter-elevation Regressions on Independent Slope Model (PRISM) with 4-km spatial resolution (www.prism.oregonstate.edu; Daly et al. 2008). We computed composites of sea surface temperature (SST) anomalies for 1900-2014 using the Hadley Centre Sea Ice and Sea Surface Temperature data set (HadISST; Rayner et al. 2003). These datasets are generated based on physically-consistent methods and models. However, due to the sparsity of observational data in the earlier part of the study period, the HadISST data have larger uncertainties (Rayner et al. 2003). The PRISM data uses observed precipitation records from the California Data Exchange Center (CDEC) stations, which has a relatively good coverage over the state since the early 1900s (Daly et al. 2008). Anomalies of wintertime vertically integrated moisture fluxes and geopotential heights at 500mb were calculated for 1901-2012 from the Twentieth Century Reanalysis Version 2 (20CR V.2; Compo et al. 2011). The 20CR V.2 data are based on assimilation of surface pressure measurements, and are also more uncertain during the early period because of the fewer number of observations. We compute the mean component of moisture fluxes from a product of monthly mean wind and specific humidity for the composite analysis during the positive and/or negative phases of the PDO and ENSO for the first and last 80 years of the record. The long-term average of the moisture fluxes is mostly driven by the mean direction and magnitude of moisture transport, while the transient eddies play a major role in moisture transport in extreme years (Kam et al. 2014a). However, as the 20C reanalysis project currently only provides monthly specific humidity and winds, we are unable to estimate the total moisture transport and convergences (mean + transient eddies). The results in section 3.2 are therefore unable to distinguish the role of transient transport and convergences to CA droughts and pluvials. To evaluate the robustness of the 20CR data, we compared regional averaged wintertime precipitation from the 20CR and PRISM data sets (temporal correlation coefficient is greater than 0.95) (see Supplementary Materials S.1).

We calculate the uncertainty of our estimates in event frequency (p) within a Bayesian framework. We choose a threshold value as the lower quartile (the 25th percentile) of California wintertime precipitation over 1901-2015 at each grid cell. For pluvials we use the upper quartile (the 75th percentile). We transform the time series of winter precipitation to a Bernoulli process, a series of zeros (no occurrence) and ones (drought or pluvial occurrences). Based on the threshold value, the expected drought or pluvial frequency ($\bar{p}$) is 0.25. We can compute the posterior distribution for the unknown parameter (p) given a Bernoulli process sample. First, we computed the lag-one autocorrelation of time series of the Bernoulli process to evaluate whether drought or pluvial years are correlated following Damsleth and El-Shaarawi (1988).

For drought and pluvial events, only one percent of the area of California shows significant autocorrelation (not shown). According to Bayesian inference theory, the posterior distribution is another beta distribution with different parameter values given the prior distribution is a uniform distribution (a beta distribution with α=1 and β=1). The posterior distributions for the full period, and the positive and negative phases of PDO, AMO, and ENSO, are derived from the fitted beta distributions that have different alpha parameters (total number of years (s) minus the number of drought occurrences (n) plus one), and different beta parameters (the number of drought occurrences plus one) during the given periods. This method follows the study of Kam et al. (2014b) that focused on drought risk over the continental US. Here, we focus on California winter meteorological drought and pluvial risk. We test the sensitivity of the impact of oceanic states on drought and pluvial risk using different moving window sizes (see S.2. in Supplementary Materials). The first and last 60 years are essentially independent (ignoring temporal persistence) but they are more sensitive to drought and pluvial events due to the relatively small window size.

To understand the impacts of global warming on drought and pluvial risk over CA, we used three GCM idealized experiment runs from the CLIVAR Drought Working Group initiative (Findell and Delworth 2009): the Geophysical Fluid Dynamics Laboratory Atmospheric Model version 2.1 (GFDM-AM2.1), the National Center for Atmospheric Research Community Climate System Model version 3.0 (CCM3.0), and the National Centers for Environmental Prediction (NCEP) Global Forecast System (GFS). Individual experiment runs were forced with prescribed idealized SST anomalies for 50 years for the GFDM-AM2.1 and CCSM3 models, and for 36 years for the GFS model, which provides larger sample sizes for combinations of the cold phase of the Pacific and the warm phase of the Atlantic than from the observational data. For example, there are only 16 years with the co-occurrence of the PDO (-), AMO (+), and ENSO (-) from the HadISST data (1900-2014). The prescribed SST patterns in the idealized experimental runs are taken from the first three modes of a rotated Principle Component Analysis (Schubert et al. 2009). The first mode is a linear trend of global sea surface temperature, the second mode is inter-annual and decadal variability of the Pacific, and the third mode is decadal variability of the Atlantic. Drought (pluvial) is defined as the 25th (75th) percentile of winter precipitation from the GCM runs forced with cold (warm) Pacific and warm (cold) Atlantic SST anomalies without global SST increasing trend. Secondly, with this threshold value, we compute the posterior distributions from the fitted beta distribution functions from the GCM experiments forced with the idealized SSTs plus global SST increasing trend. This enables us to quantify changes in drought and pluvial risk due to the SST increasing trend as depicted by the models.

3. Results

3.1. The Changing Influence of Oceanic States on California Drought and Pluvial Risk

Our results indicate that over California a strong negative phase of the PDO has historically increased the expected drought frequency by more than 5% (frequency=0.3; return period of about three years) while a strong positive phase decreased it by 5%. The cool La Niña phase of the ENSO increased the expected drought frequency over southern California by more than 5% regardless of its strength; however strong positive events (El Niño) decreased drought frequency over all California by 10% (frequency=0.15; return period of about six years) (Figure 2 d-e). The AMO, by itself, plays a minor role in California wintertime drought. These oceanic influences have likely played a role in the recent California drought. During the winters of 2011/12 and 2012/13, the cool La Niña phase of ENSO persisted, and the cold phase of the PDO and the warm phase of the AMO persisted during the winter of 2011/12 through the fall of 2013, which led to winter precipitation deficits below 25th percentile during these winters.

Since February 2014, the PDO, AMO, and ENSO have been in transition, with precipitation slightly more than the 25th percentile during the winter of 2014-15.

We find that in recent decades, the influence of SSTs on California drought has changed. During the last 80 years (1936-2015), the negative phases of ENSO and PDO are associated with an elevation of the risk of drought for 40% and 32% of the area of California, respectively, with probability ≥ 0.9 (hatched areas in Figure 3), while less than 5% of the area of California showed elevated drought risk during these phases of ENSO and PDO over the first 80 winters (1901-1980). In contrast, there has been no significant change in overall drought risk, irrespective of oceanic states. The positive phase of the AMO elevated the risk of drought moderately between the first 80 and last 80 years (only 6% of the region; not shown). This suggests that the spatial patterns of the influence of the PDO (-) and ENSO (-) and their impacts on California winter drought have changed at multi-decadal scale. The positive phases of the PDO and ENSO are associated with increased winter pluvial risk over the whole of California, and northern California, respectively. Changes in pluvial risk between the two periods (1901-1980 and 1936-2015) are significant but for a smaller area relative to the changes in drought risk (7-8% of the region shows a significant increase in pluvial risk and no areas show a significant decrease; Figure 3).

3.2. Potential Mechanisms of Changes in California Drought and Pluvial Risk

Composite annual SST anomaly patterns for the last 80 years show that the surface temperature gradient between the northcentral and equatorial Pacific has become larger for both the PDO (-) and ENSO (-). Specifically, warm SST anomalies during the negative phase of the PDO have become significantly warmer over the northcentral Pacific compared to the first 80 years (based on the t-test at a significance level = 0.05 darker red and hatched area in Fig. 4 (c)). Over the same period, cool SST anomalies during the negative phase of the ENSO have become cooler over the tropical Pacific with statistically significant changes over the equatorial Pacific region. Although global warming contributed to the emergence of positive sea surface temperature anomalies over most of the Pacific Ocean during this time period, the magnitude of these anomalies are relatively weak compared to the changes in the anomalies over the regions related to the PDO and ENSO (see S.3 in Supplementary Materials).

The changes in the SST anomaly patterns are associated with changes in large-scale atmospheric circulation over tropical and extra-tropical regions of the Pacific (Figure 4). During the last 80 years, weaker northwesterly winds over the north Pacific have occurred during the PDO (-) phase, resulting in less southeastward moisture transport. Similarly, stronger easterly winds over the equatorial Pacific, have occurred during the ENSO (-) phase, resulting in greater westward moisture transport. These moisture transport patterns reduce precipitation over California more than normal. Conversely, this led to more moisture convergence (above-normal precipitation) over the western Pacific and southeast Asia. This mechanism is consistent with idealized model experiments. Over the extra-tropical Pacific region, cold and warm SST anomalies (above two standard deviations) over the tropical and northcentral Pacific via air-sea interactions (Lau and Nath 1996) induced high pressure in the mid-troposphere during the PDO (-) phase, which caused less moisture transport equatorward from the northcentral Pacific. These anomalies were stronger during 1934-2011 compared to 1901-1980 (see S.4 in Supplementary Materials), thus increasing the risk of drought during the PDO (-) and ENSO (-). For pluvial events, the PDO (+) and ENSO (+) phases show statistically significant positive SST anomalies over a broader region of the tropical Pacific during the last 80 years (see S. 5 in Supplementary Materials) than the PDO (-) and ENSO (-) phases. These anomalies drove moisture transport over the tropical region in the opposite direction and thus more pluvial events over northern California. Examination of changes in risk over the broader region of the Western U.S. (Figure 5) shows that decreased moisture transport over southern California and increased moisture transport over northern California are embedded in an overall northward shift in pluvial risk and southward shift in drought risk.

To test whether climate change has played a role in changing the risk of California winter droughts and pluvials, we compared idealized SST experiment simulations of three global climate models and without global SST increasing trend as one of the results due to climate change (Figure 6). Without the SST increasing trend, the model experiments show that cold SST anomalies over the Pacific and warm SST anomalies over the north Atlantic (similar to a combination of the PDO (-), AMO (+), and ENSO (-)) are associated with reduced precipitation over the U.S. southwest, indicating that the models can reproduce the observed relationships between oceanic states and California precipitation variability. With the global SST increasing trend, the models show decreases in the precipitation deficit induced by cold Pacific and warm Atlantic SSTs, and decreases in precipitation surplus induced by warm Pacific and cold Atlantic SSTs, suggesting an overall weakening of the intensity of SST-driven wintertime extremes. There is some disagreement of the GCM responses to global SST warming trends in terms of the spatial patterns over California, but the models show a fairly consistent response (e.g. reduction of precipitation deficits) to the warming trends at regional scale. Based on available data for a single climate model with an historic climate simulation, the global SST increasing trend has slightly offset increases in drought (pluvial) risk induced by cold (warm) Pacific SSTs, but not significantly (see S.6 in Supplementary Materials).

4. Conclusion and Outlook for California Drought Risk

The longevity and severity of the 2011-2015 California winter drought have implicated climate change as having played a role. However, this drought should be viewed in the context of multi-decadal climate variability, and in particular changes in oceanic states associated with ENSO and the PDO that provide ideal conditions for drought. Idealized model experiments suggest that the increase in drought and pluvial risk over much of California during favorable oceanic phases is mainly due to natural variability, although global warming may have offset these increases somewhat.

Since the winter of 2014/2015 the ENSO and PDO have transitioned to their positive phases, which are associated with an increase in wintertime pluvial risk over California. Climate model predictions indicate that the positive ENSO phase will persist through to 2016 (Kirtman et al. 2014) with the expectation of a precipitation surplus in the winter of 2015/16, which might help alleviate the current drought. However, decadal forecasts initialized with observed wind stresses (Thoma et al. 2015) predict that the current negative PDO conditions (also associated with the global warming hiatus (Delworth et al. 2015)) will persist until the mid-2020s, suggesting that the long-term risk of drought over California will continue to be elevated, with the occurrence of individual drought events depending on the frequency of ENSO (-) (La Niña) events.

Acknowledgements

We are grateful to Dr. Ming Pan and Dr. Kirsten Findell for sharing the simulated snow water equivalent data and the idealized SST experiment runs. This work was partly funded by NOAA grants NA14OAR4310218, NA10OAR4310130 and NA11OAR4310097.

References

Barnett, et al., 2008, Human-induced changes in the hydrology of the Western United States, Science, **319**, 1080-1083.

Bond, N. A., M. F. Cronin, and N. Mantua, 2015, Causes and impacts of the 2014 warm anomaly in the NE Pacific, *Geophys. Res. Lett.*, **42**, 3414-2420.

Compo et al. 2011, The Twentieth Century Reanalysis Projects, *Q. J. R. Meteorol. Soc.*, **137**, 1-28.

Cook, B. I., Smerdon, J. E., Seager, R., and Cook, E. R., 2014, Pan-continental droughts in North America over the last millennium, *J. Climate.*, **27**, 383-397.

Daly et al., 2008, Physiographically sensitive mapping of climatological temperature and precipitation across the conterminous United States, *Int. J. Climatol.*, **28**, 2031-2064.

Damsleth, E. and A. H. El-Shaarawi, 1988, Estimation of autocorrelation in a binary time series, *Stochastic Hydrol. Hydraul.*, **2**, 61-72.

Delworth et al., 2015, A Link between the Hiatus in Global Warming and North American Drought. *J. Climate*, **28**, 3834–3845.

Dixon, L. S., Moore, N. Y., and Pint, E. M., 1996, Drought management policies and economic effects in urbarn areas of California, 1987-1992, RAND.

Famiglietti, et al., 2011, Satellite measure recent rates of groundwater depletion in California's Central Valley, Geophys. Res. Lett., 38, L03403.

Findell, K. L., Delworth T. L., 2009, Impact of common sea surface temperature anomalies on global drought and pluvial frequency, *J. Climate*, **23**, 485-503.

Gimeno, et al., 2012, Oceanic and terrestrial sources of continental precipitation, *Rev. Geophys.*, **50**, RG4003.

Grantham, T. E., and J. H. Viers, 2014, 100 years of California's water rights system: patterns, trends, and uncertainy, *Environ. Res. Lett.*, **9**, 084012.

Kam, J., J. Sheffield, and E. F. Wood, 2014a, A multi-scale analysis of drought and pluvial mechanisms for the southeastern United States, J. Geophys. Res. Atmos., **119**, 7348-7367.

Kam, J., J. Sheffield, and E. F. Wood, 2014b, Changes in drought risk over the contiguous United States (1901-2012): The influence of the Pacific and Atlantic Oceans, *Geophys. Res. Lett.*, **41**, 5897-5903.

Kam, J., T. R. Knutson, F. Zeng, and A. T. Wittenberg, 2015, Record annual-mean warmth over Europe, the northeast Pacific, and the northwest Atlantic during 2014: Assessment of anthropogenic influence ["Explaining extreme events of 2014 from a climate perspective"], *Bull. Amer. Meteor. Soc.*, **96**, S61-65.

Kirtman, et al., 2014, The North American Multimodel Ensemble: Phase-1 Seasonal-to-Interannual Prediction; Phase-2 toward Developing Intraseasonal Prediction. *Bull. Amer. Meteor. Soc.*, **95**, 585–601.

Lau N.-C. and M. J. Nath, 2009, The Role of the "Atmospheric Bridge" in Linking Tropical Pacific ENSO Events to Extratropical SST Anomalies. *J. Climate*, **9**, 2036–2057.

Mao, Y., B., Nijssen, and D. P. Lettenmaier, 2015, Is climate change implicated in the 2013/14 California drought? A hydrologic perspective, Geophys. Res. Lett., **42**, 205-2813.

McCabe, G. J., M. A. Palecki, and J. L. Betancourt, 2004, Pacific and Atlantic Ocean Influences on multidecadal drought frequency in the United States. *Proc. Natl. Acad. Sci. USA*, **101**, 4136-4141.

Mo. K. C., Schemm, J., and Yoo, S., 2009, Influence of ENSO and the Atlantic Multidecadal oscillation on drought over the United States, *J. Climate*, **22**, 5962-5982.

Namias, J., 1978, Recent drought in California and western Europe, *Rev. Geophys.*, **16**, 435–458.

Pan et al., 2003, Snow process modeling in the North America Land Data Assimilation System

(NLDAS): 2. Evaluation of model simulated snow water equivalent, *J. Geophys. Res.*, **108**, 8850.

Rayner et al., 2003, Global analyses of sea surface temperature, sea icea, and night marine air temperature since the late nineteenth century, J. Geophys. Res., **108**, 4407

Seager, R. et al., 2007, Model projections of an imminent transition to a more arid climate in Southwestern North America, Science, 316, 1181-1184.

Seager R., et al., 2015, Causes of the 2011 to 2014 California drought, *J. Climate*., **28**, 6997–7024.

Schonher, T. and S. E. Nicholson, 1989, The Relationship between California Rainfall and ENSO Events. *J. Climate*, **2**, 1258–1269.

Schubert et al., 2004, On the cause of the 1930s Dust Bowl, *Science*, **303**, 1855-1859.

Stine, S., 1994, Extreme and persistent drought in California and Patagonia during mediaeval time, *Nature*, **269**, 546-549.

Thoma et al., 2015, Decadal hindcasts initialized using observed surface wind stress: Evaluation and Prediciton out to 2024, Geophys. Res. Lett., **42**, 6454–6461.

Wang, H., Schubert, S., 2014, Causes of the extreme dry conditions over California during early 2015 in ["Explaining extreme events of 2013 from a climate perspective"], Bull. Am. Meteorol. Soc., 95, S7–S11.

Captions of Figures

Figure 1: The severity of 2014-15 California drought. (a) Simulated snow water equivalent percentile is simulated from the Variable Infiltration Capacity (VIC) land surface hydrologic model. The percentile is computed with respect to the samples within a 49-day window in 1951-2004. (b) Time series of water thickness anomalies over May 2002 throughApril 2015 from the GRACE data, which is based on the climatology 2004-2008. The GRACE data shows the deficit of water storage is about -4.0 cm on November 1 in 2013 (the water storage deficit in November based on climatology (2004-2008) is -2.0 cm). (c-f) Time series of winter precipitation (c), annual Pacific Decadal Oscillation (PDO) index (d), Atlantic Multi-decadal Oscillation (AMO) index (e), and Southern Oscillation Index (SOI) over 1900-2014. The medians of winter time precipitation are represented in (c). The positive phase of SOI represent a La Niña (negative) phase of El-Niño Southern Oscillation (ENSO).

Figure 2: Favorable oceanic conditions for California drought. Time series of the monthly PDO (a), AMO (b), and ENSO (c) from January 2011 through February 2015. d-e) The conditional distributions are computed from the regional averages of drought occurrences during the certain times: strong negative (blue; below the 33rd percentiles), negative (sky; below the medians), climatology (black; 1900-2014), positive (orange; above the medians), and strong positive (red; above the 66th percentiles) of the annual PDO, AMO, and ENSO indices, respectively. The bottom and top of the box stand for the accumulated belief of degree at 25% and 75% from the inverse posterior distribution functions and the band within the box, the accumulated belief degree at 50% from the inverse posterior distribution functions. Whiskers represent the accumulated belief degree at 1% and 99% from the inverse posterior distribution functions. North and south California are defined above and below 37.5°N.

Figure 3: Multi-decadal changes in the Pacific Ocean with California winter drought and pluvial risk. Drought frequency maps during the negative phases of the PDO and ENSO indices of the periods, 1901-1980 (a-b) and 1936-2015 (d-e). Pluvial frequency maps during the positive phases of the PDO and ENSO indices of the periods, 1901-1980 (g-h) and 1936-2015 (j-k). To address the trends in drought and pluvial risk, drought and pluvial frequency maps during the first and last 80 years periods are in the last column (c, f, i, and l). Green shaded areas represent the area with the uncertainty equal to or greater than the probability equal to or greater than 90%, to have higher drought and pluvial frequency than 0.25 (DB{$p \geq 0.25$}) based on the conditional posterior distributions.

Figure 4: Multi-decadal changes in the Pacific Ocean and their associations with moisture transport and convergences. Composite spatial distributions for annual averaged sea surface temperature anomalies during the PDO (-) and ENSO (-) phases of the periods, 1901-1980 (a-b) and 1935-2014 (c-d). Composite spatial distributions for wintertime vertically integrated moisture transport and convergence anomalies during the anomalies during the negative phases of the PDO and ENSO indices of the periods, 1900-1979 (e-f) and 1936-2012 (g-h).

Figure 5: Multi-decadal changes in winter drought and pluvial risk over the western U.S. for different phases of SST variations in the Pacific Ocean. Green shaded areas over blue (red) colored areas represent areas with higher drought and pluvial frequency than 0.25 (DB{$p \geq 0.25$}) based on the conditional posterior distributions with probability equal to or greater than 90% (smaller than 10%).

Figure 6: Idealized SST experiment runs of global climate models from the Climate Variability and Predictability (CLIVAR) Drought Working Group initiative: the Geophysical Fluid Dynamics Laboratory Atmospheric Model version 2.1 (GFDM-AM2.1), the National Center for Atmospheric Research Community Climate System Model version 3.0 (CCM3.0), and the National Centers for Environmental Prediction (NCEP) Global Forecast System (GFS). Here,

four different SST experiments from three GCM are represented; cold Pacific and warm Atlantic SST anomalies without/with long-term global warming (cPwA and cPwAwT, respectively), and warm Pacific and cold Atlantic SST anomalies without/with long-term global warming (wPcA and wPcAwT, respectively). For each SST experiments, GFDL-AM2.1 and CCM3 are 50-year simulations and GFS is 36-year simulations. The differences of winter precipitation are computed from the average over the full period from an individual experiment run.

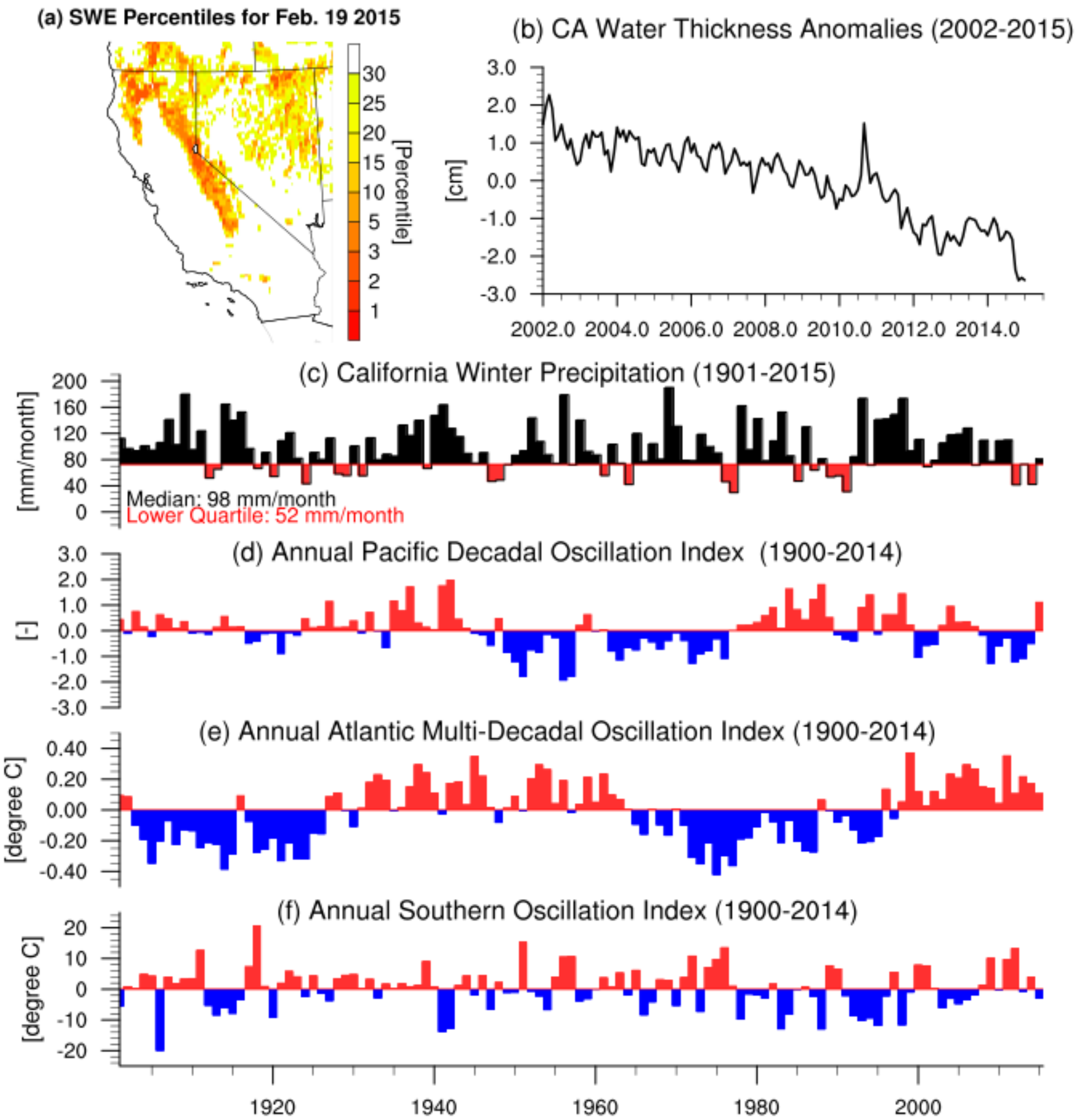

Figure 1. The severity of 2014-15 California drought. (a) Simulated snow water equivalent percentile is simulated from the Variable Infiltration Capacity (VIC) land surface hydrologic model. The percentile is computed with respect to the samples within a 49-day window in 1951-2004. (b) Time series of water thickness anomalies over May 2002 throughApril 2015 from the GRACE data, which is based on the climatology 2004-2008. The GRACE data shows the deficit of water storage is about -4.0 cm on November 1 in 2013 (the water storage deficit in November based on climatology (2004-2008) is -2.0 cm). (c-f) Time series of winter precipitation (c), annual Pacific Decadal Oscillation (PDO) index (d), Atlantic Multi-decadal Oscillation (AMO) index (e), and Southern Oscillation Index (SOI) over 1900-2014. The medians of winter time precipitation are represented in (c). The positive phase of SOI represent a La Niña (negative) phase of El-Niño Southern Oscillation (ENSO).

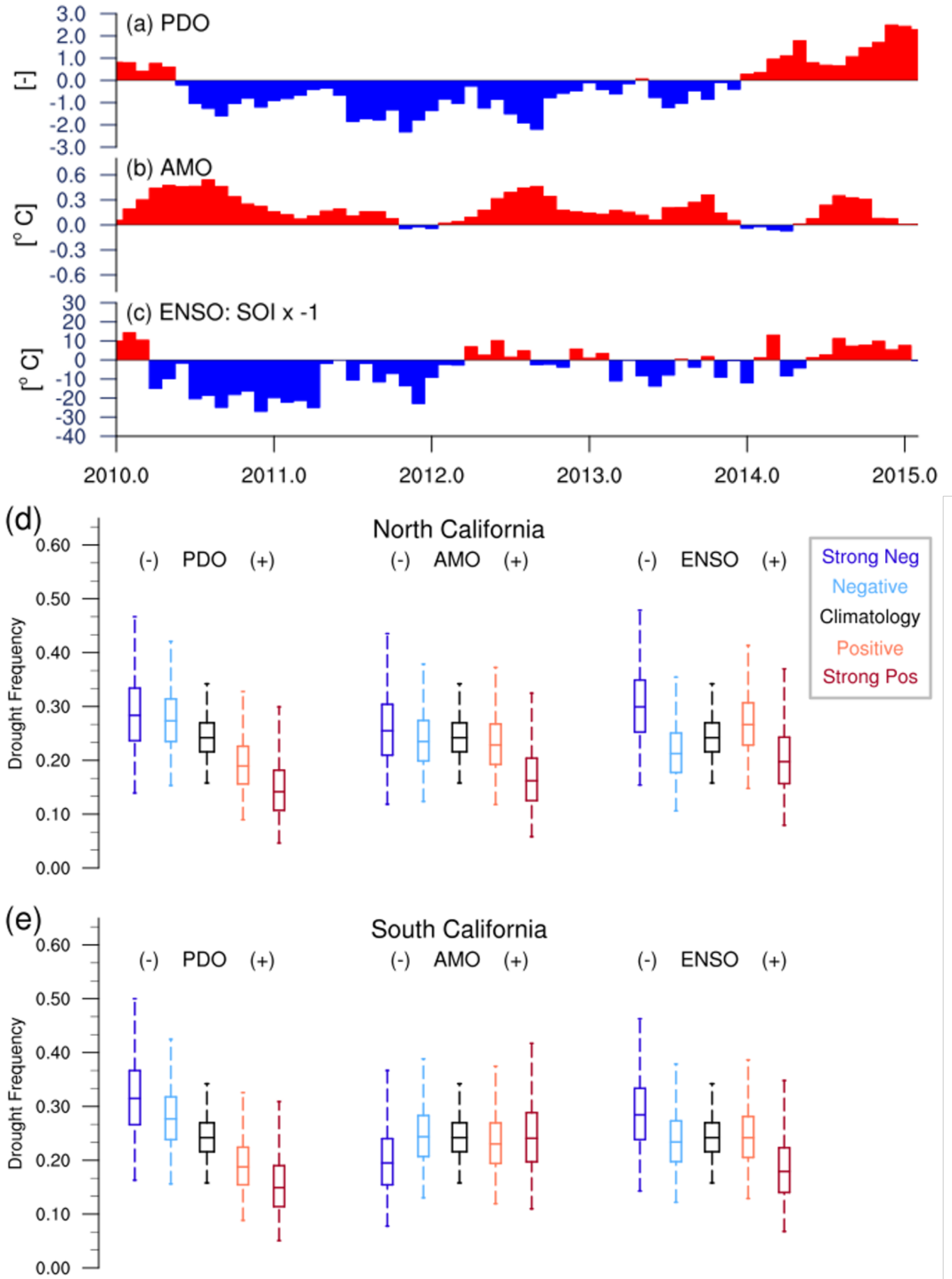

Figure 2: Favorable oceanic conditions for California drought. Time series of the monthly PDO (a), AMO (b), and ENSO (c) from January 2011 through February 2015. d-e) The conditional distributions are computed from the regional averages of drought occurrences during the certain times: strong negative (blue; below the 33rd percentiles), negative (sky; below the medians), climatology (black; 1900-2014), positive (orange; above the medians), and strong positive (red; above the 66th percentiles) of the annual PDO, AMO, and ENSO indices, respectively. The bottom and top of the box stand for the accumulated belief of degree at 25% and 75% from the inverse posterior distribution functions and the band within the box, the accumulated belief degree at 50% from the inverse posterior distribution functions. Whiskers represent the accumulated belief degree at 1% and 99% from the inverse posterior distribution functions. North and south California are defined above and below 37.5°N.

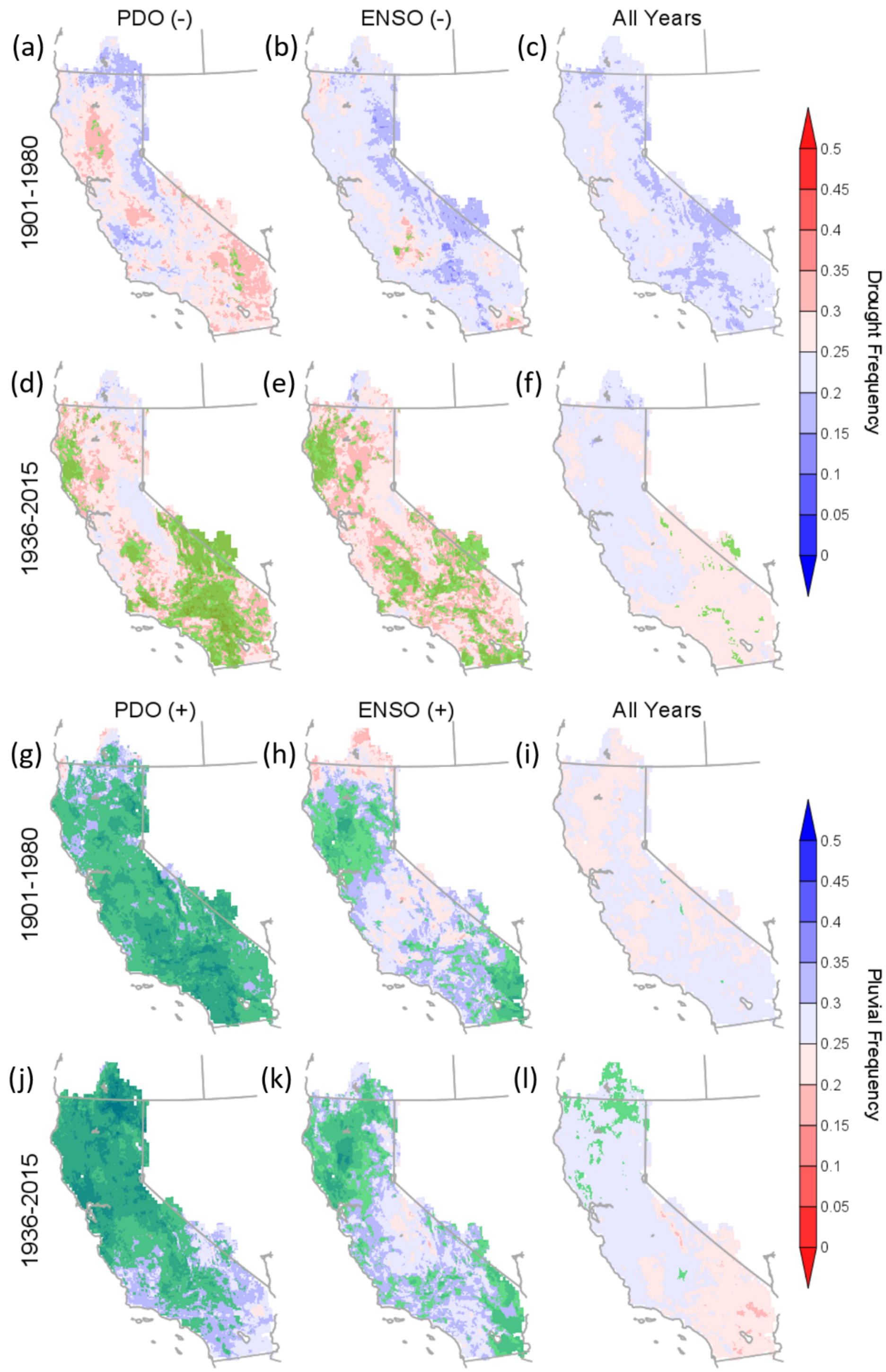

Figure 3: Multi-decadal changes in the Pacific Ocean with California winter drought and pluvial risk. Drought frequency maps during the negative phases of the PDO and ENSO indices of the periods, 1901-1980 (a-b) and 1936-2015 (d-e). Pluvial frequency maps during the positive phases of the PDO and ENSO indices of the periods, 1901-1980 (g-h) and 1936-2015 (j-k). To address the trends in drought and pluvial risk, drought and pluvial frequency maps during the first and last 80 years periods are in the last column (c, f, i, and l)Green shaded areas represent the area with the uncertainty equal to or greater than the probability equal to or greater than 90%, to have higher drought and pluvial frequency than 0.25 (DB{$p \geq 0.25$}) based on the conditional posterior distributions.

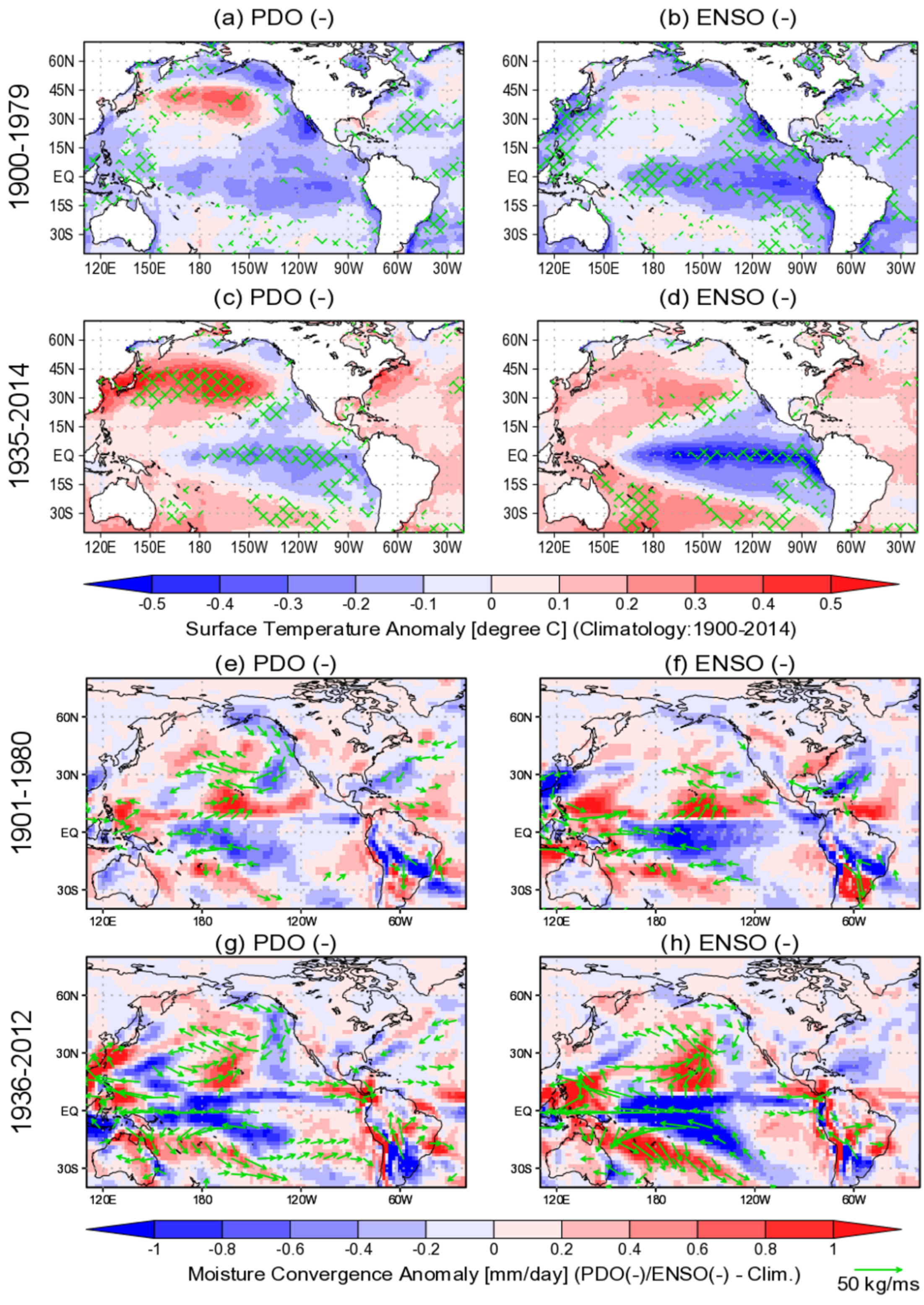

Figure 4: Multi-decadal changes in the Pacific Ocean and their associations with moisture transport and convergences. Composite spatial distributions for annual averaged sea surface temperature anomalies during the PDO (-) and ENSO (-) phases of the periods, 1901-1980 (a-b) and 1935-2014 (c-d). Composite spatial distributions for wintertime vertically integrated moisture transport and convergence anomalies during the anomalies during the negative phases of the PDO and ENSO indices of the periods, 1900-1979 (e-f) and 1936-2012 (g-h).

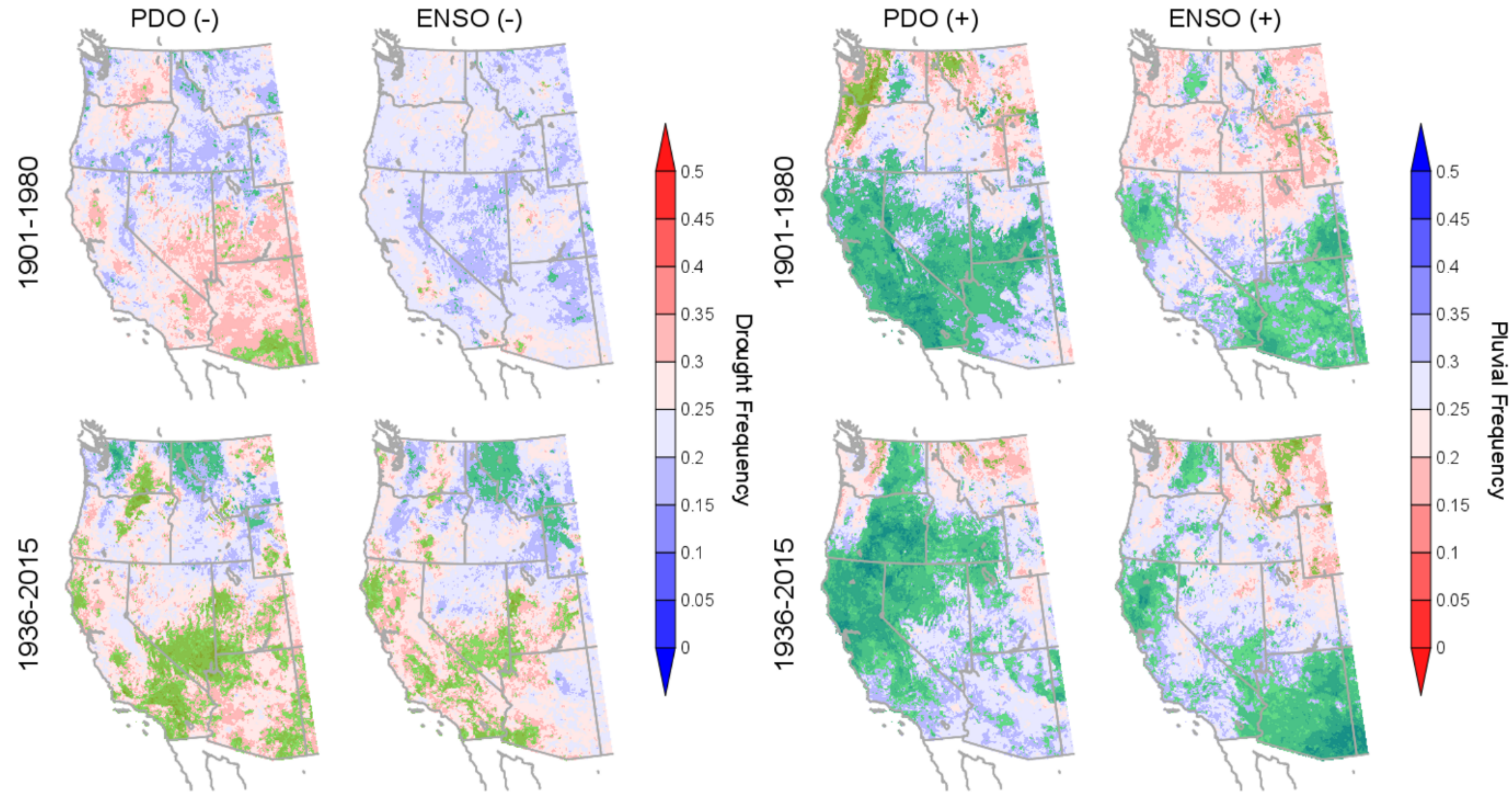

Figure 5: Multi-decadal changes in winter drought and pluvial risk over the western U.S. for different phases of SST variations in the Pacific Ocean. Green shaded areas over blue (red) colored areas represent areas with higher drought and pluvial frequency than 0.25 (DB{p ≥ 0.25}) based on the conditional posterior distributions with probability equal to or greater than 90% (smaller than 10%).

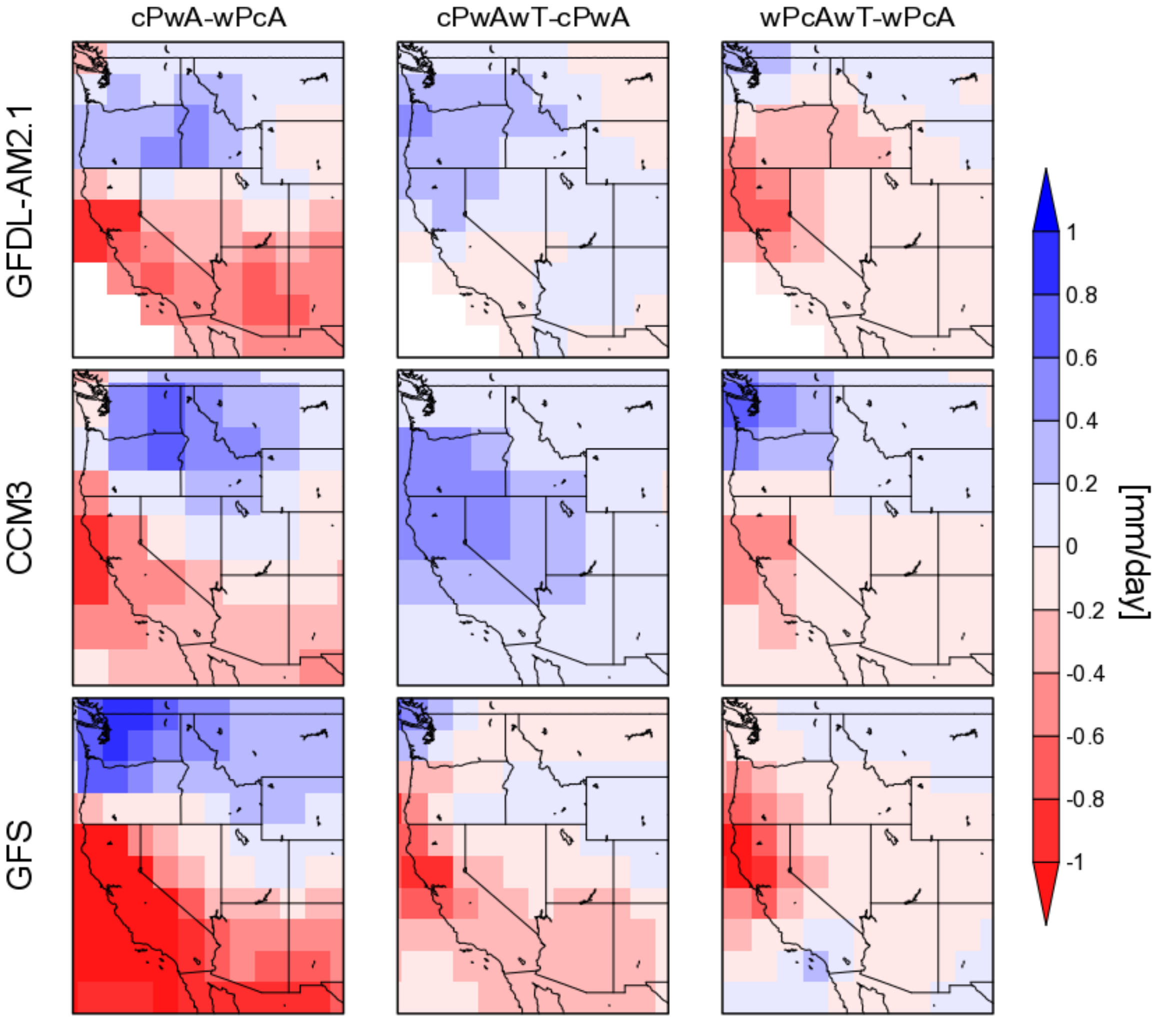

Figure 6: Idealized SST experiment runs of global climate models from the Climate Variability and Predictability (CLIVAR) Drought Working Group initiative: the Geophysical Fluid Dynamics Laboratory Atmospheric Model version 2.1 (GFDM-AM2.1), the National Center for Atmospheric Research Community Climate System Model version 3.0 (CCM3.0), and the National Centers for Environmental Prediction (NCEP) Global Forecast System (GFS). Here, four different SST experiments from three GCM are represented; cold Pacific and warm Atlantic SST anomalies without/with long-term global warming (cPwA and cPwAwT, respectively), and warm Pacific and cold Atlantic SST anomalies without/with long-term global warming (wPcA and wPcAwT, respectively). For each SST experiments, GFDL-AM2.1 and CCM3 are 50-year simulations and GFS is 36-year simulations. The differences of winter precipitation are computed from the average over the full period from an individual experiment run.